Accepted Manuscript

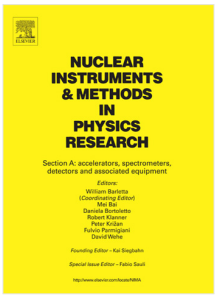

A conceptual solution for a beam halo collimation system for the Future Circular hadron–hadron Collider (FCC-hh)

M. Fiascaris, R. Bruce, S. Redaelli

PII: S0168-9002(18)30375-9
DOI: https://doi.org/10.1016/j.nima.2018.03.042
Reference: NIMA 60684

To appear in: *Nuclear Inst. and Methods in Physics Research, A*

Received date : 30 November 2017
Revised date : 28 February 2018
Accepted date : 10 March 2018

Please cite this article as: M. Fiascaris, R. Bruce, S. Redaelli, A conceptual solution for a beam halo collimation system for the Future Circular hadron–hadron Collider (FCC-hh), *Nuclear Inst. and Methods in Physics Research, A* (2018), https://doi.org/10.1016/j.nima.2018.03.042

A conceptual solution for a beam halo collimation system for the Future Circular hadron-hadron Collider (FCC-hh)

M. Fiascaris[1], R. Bruce, S.Redaelli

CERN, Geneva, Switzerland

Abstract

We present the first conceptual solution for a collimation system for the hadron-hadron option of the Future Circular Collider (FCC-hh). The collimation layout is based on the scaling of the present Large Hadron Collider collimation system to the FCC-hh energy and it includes betatron and momentum cleaning, as well as dump protection collimators and collimators in the experimental insertions for protection of the final focus triplet magnets. An aperture model for the FCC-hh is defined and the geometrical acceptance is calculated at injection and collision energy taking into account mechanical and optics imperfections. The performance of the system is then assessed through the analysis of normalized halo distributions and complete loss maps for an ideal lattice. The performance limitations are discussed and a solution to improve the system performance with the addition of dispersion suppression collimators around the betatron cleaning insertion is presented.

Keywords: FCC-hh; collimation; aperture; tracking simulations.

1. Introduction

The hadron-hadron option of the Future Circular Collider study, FCC-hh [1, 2], is designed to provide *pp* collisions at a centre of mass energy of 100 TeV. For a nominal total beam intensity of about 10^{15} protons, the total stored energy per beam will be about 8500 MJ, a factor of 24 above that of the CERN Large Hadron Collider (LHC) [3]. The high energies and intensities required at the FCC-hh pose daunting challenges on the control of beam losses. Its beams are highly destructive: uncontrolled losses of even just a small fraction of the beam can cause a magnet to quench or damage to accelerator components, both at injection (3.3 TeV) and even more at collision (50 TeV) energy.

A collimation system is needed to intercept and safely dispose of unavoidable beam losses. Its main functionalities are: efficient cleaning of the beam halo ensuring an operation safely below quench limits both at injection and top energy; passive protection of the machine aperture against abnormal losses

and minimisation of the halo-induced experimental backgrounds. In this paper, only beam halo cleaning is considered since this is expected to be the driving constraint for the FCC-hh collimation system. At the LHC this is achieved through a multi-stage cleaning [3, 4, 5, 6, 7, 8] with two dedicated insertions for betatron and momentum collimation. Given the excellent performance of the LHC collimation system, validated up to energies of 6.5 TeV and stored beam energy of about 300 MJ [9, 10], the first conceptual solution for the FCC-hh collimation is a scaled-up system derived from the present LHC design. This conservative, yet solid approach, allows us to evaluate the achievable performance with the current state-of-the-art technology and to start a mechanical design based on a first assessment of power loads. Further improvements and technological developments will be considered at a later stage.

In this paper, the focus is on aspects related to the cleaning performance with the aim of setting up the work flow necessary to achieve a complete system design. The target cleaning performance can be achieved by optimizing the collimation system layout and the collimator settings. Related to the latter is the geometrical aperture of the machine. A detailed knowledge of the aperture margins in the machine is in fact necessary to ensure that all elements, in particular the super-conducting ones, are protected by the collimation system. The work flow of collimation studies includes therefore several iterations of machine aperture calculations and tracking simulations to optimize the collimator settings and the system layout. Information on unprotected elements is also fed back to review either the magnets' physical apertures or the collimator settings. The scope of this paper is to demonstrate this work flow through a first complete iteration. The results of the studies presented here also serve as input for detailed energy deposition simulations and thermo-mechanical analyses, such as those presented in [11], which are necessary to achieve the collimator hardware design.

The paper is organised as follows. First, the design goals of the FCC-hh collimation system and key parameters for the system specifications are presented. After a description of the new system's layout and optics, baseline collimator settings are proposed. The aperture of the FCC-hh is then reviewed at injection and collision energy. The results of detailed particle tracking simulations are then presented and the performance of the system at injection and collision energy is assessed through the analysis of proton loss maps.

2. FCC-hh collimation design goals

The performance of the collimation system is described by the cleaning inefficiency η_c, defined as the ratio of surviving halo protons N_p with a normalized betatron amplitude A above a given amplitude A_0 to the number of protons absorbed by the collimation system (N_{abs}) [12, 13, 14]:

$$\eta_c(A_0) = \frac{N_p(A > A_0)}{N_{abs}}. \quad (1)$$

Losses are distributed longitudinally around the ring. It is therefore useful to define a local cleaning inefficiency $\tilde{\eta}_c$ which is a function of the longitudinal coordinate s and has units of 1/m. Detailed tracking simulations are used to predict $\tilde{\eta}_c$ along the accelerator with a resolution determined by the bin size Δs:

$$\tilde{\eta}_c(s) = \frac{1}{\Delta s} \cdot \frac{N_{\mathrm{loss}}(s \rightarrow s + \Delta s)}{N_{\mathrm{abs}}}, \tag{2}$$

where $N_{\mathrm{loss}}(s \rightarrow s + \Delta s)$ is the number of particles lost on the mechanical aperture between position s and $s + \Delta s$.

Beam loss mechanisms result in a decay of the beam intensity N with time t, usually characterised by an exponential decay with the beam lifetime τ_b as decay constant:

$$N(t) = N_0 e^{-\frac{t}{\tau_b}}. \tag{3}$$

τ_b varies during operation. The collimation system must be designed to cope with the maximum expected rates of beam losses, which are described by the minimum allowed beam lifetime τ_b^{min}. In addition to the minimum allowed beam lifetime, the key parameters that determine the target performance of a collimation system are the beam intensity and the quench level R_q, given here in units of protons/m/s. To leading order of Eq. (3), these quantities are related to collimation cleaning inefficiency by the following equation, which describes the condition for operating the machine while ensuring that losses in the cold magnets remain below the quench limit:

$$\frac{N}{\tau_b^{min}} \times \tilde{\eta}_c < R_q. \tag{4}$$

While a detailed assessment of the cleaning performance requires more complete energy deposition studies at critical loss locations, this formalism based on estimates of the protons lost on the accelerator aperture is well suited for a first system design and performance optimization.

The relevant parameters for the FCC-hh are summarised in Table 1. The minimum allowed beam lifetimes at injection and top energy are assumed to be the same as for the LHC. Detailed quench limits for FCC-hh magnets are not yet available, however, the quench level has been estimated at $R_q = 0.5 \times 10^6$ p/m/s at 50 TeV [15] by scalings from the LHC. It is first assumed that the FCC magnets have the same quench limit, in terms of power load per volume, at 50 TeV as the LHC magnets at 7 TeV, which is around 5 mW/cm^3. Then, the LHC design value of $R_q = 7.8 \times 10^6$ p/m/s at 7 TeV [16, 14] is scaled down by the approximated increase in peak power density per proton at 50 TeV [16], and the above estimate for R_q is obtained.

Substituting this values into Eq. (4) and assuming $\tau_b^{min} = 0.2$ h, the LHC design value, the required cleaning inefficiency at 50 TeV is calculated to be 3×10^{-7} m^{-1}. In the absence of more accurate estimates, this target value will be taken as a benchmark to assess the performance of the collimation system in Sec. 6.3. Given that the performance requirements are most stringent at collision

energy, a solution for 50 TeV energy is also expected to fulfill the requirements at injection energy.

Table 1: Beam parameters and assumptions on the minimum allowed beam lifetime for the FCC-hh at injection and collision energy. Bunch parameters are given for 25 ns bunch spacing.

	FCC-hh		**LHC design**
	Injection	Collision	Collision
Beam energy [TeV]	3.3	50	7
Number of bunches (at 25 ns)	10600	10600	2808
Bunch population (at 25 ns)	$1 \cdot 10^{11}$	$1 \cdot 10^{11}$	$1.15 \cdot 10^{11}$
Beam intensity (N_{tot})	$1.06 \cdot 10^{15}$	$1.06 \cdot 10^{15}$	$3 \cdot 10^{14}$
Stored energy [MJ]	560	8500	360
Assumed minimum beam lifetime (τ_b^{min})	0.1 h	0.2 h	0.2 h
Beam loss power load ($t = \tau_b^{min}$) [MW]	1.6	11.8	0.5

The maximum energy load on the collimators from beam losses must also be estimated for an appropriate design of the system. The choice of jaw material and the hardware design must ensure the robustness and the mechanical stability of the collimators. For the given loss assumptions and beam parameters, the power load at collision energy amounts to 11.8 MW. Even if beam losses occur locally at one collimator, the deposited power is only partially dissipated on its jaws. Due to the development of hadronic and electromagnetic showers, most of the power is absorbed on downstream elements. The tracking simulations presented in this paper do not account for secondary shower development and therefore this aspect is not treated here. Detailed energy deposition studies and thermo-mechanical analyses, such as those presented in [11], will be necessary to complete the system design work flow and achieve a first collimator hardware design.

The complete design must also take into account the interplay between different parameters and constraints. For instance, excessive impedance must be avoided by an appropriate choice of collimator settings (which determine the opening of the collimators in mm) and jaw material. Beam loads on the collimators for given loss assumptions are used as inputs to design the collimators and also to assess yearly radiation doses to components in the collimation areas. This information is then fed back to the design of the underground areas (access constraint, design of service galleries and infrastructures, ...). These aspects will be addressed in future iterations of this conceptual system design.

3. Baseline layouts of the FCC-hh collimation system

The studies presented in this paper were performed with lattice version 7 of the FCC-hh layout [17] described in Table 1 and shown in Figure 1 [18]. This layout was adopted as the baseline for FCC-hh until November 2016, when an improved version was introduced, and was used for the first FCC-hh design

studies such as the one presented here. This layout includes two insertions for the high-luminosity interaction points (IPs) A and G, and two insertions for the low-luminosity IPs F and H. For the high-luminosity IPs, the optics design is characterised by $L^\star = 45$ m and $\beta^\star = 0.3$ m, where $L^\star$ is defined as the distance from the IP to the start of the triplet and $\beta^\star$ is the value of the optical β-function at the IP. The optics for the low-luminosity IPs are not yet defined, hence insertions IPF and IPH are made of simple transfer lines. Therefore, in the rest of the paper, the term IP will refer exclusively to the high-luminosity insertions, IPA and IPG. The FCC-hh ring is made of four short arcs, eight long arcs , six short straight sections and two long (also called extended) straight sections. Betatron and momentum cleaning are performed in two separate insertions. The so called Extended Straight Section D (ESS-D) is dedicated to the beam extraction followed by betatron collimation on the clock-wise beam (referred to as Beam 1, or B1, as in the LHC notation), while momentum collimation is performed on the counter-rotating beam (Beam 2, or B2). Similarly, in the ESS-J momentum cleaning is performed on B1 and extraction followed by betatron collimation on B2. The optics seen by both beams are the same by design. In the rest of this paper we will thus consider B1 only as our study case, therefore it is assumed that betatron cleaning is implemented in ESS-D and momentum cleaning in ESS-J.

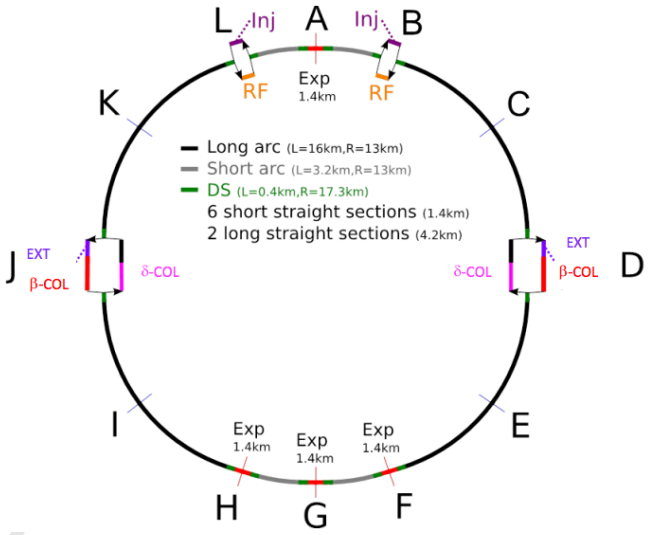

Figure 1: Schematic layout of the FCC-hh, as of October 2016, with the configuration of the extraction, off-momentum and betatron collimation in the extended straight sections D and J.

The optics functions for betatron cleaning are shown in Figure 2 (top). They are similar to those optimized for the halo collimation in LHC, except that they are scaled up by a factor $k_\beta = 5$, resulting in an insertion length of 2.7 km. The scaling factor was chosen to achieve collimator gaps that are similar to

Table 2: Parameters of the FCC-hh ring. The lattice v7 [19] was used. The scale factor for the cleaning betatron, k_β, and off-momentum, k_p, insertions refers to the factor used to scale the betatron functions from the LHC to the FCC-hh. For the interaction region, the ultimate $\beta^\star$ value at 50 TeV energy is indicated.

Parameter	**Value**
Circumference	100.171 km
Betatron cleaning insertion:	
Scale factor k_β	5
Length	2.7 km
Momentum cleaning insertion:	
Scale factor k_p	2.7
Length	1.4 km
Interaction regions:	
$\beta^\star$	0.3 m
$L^\star$	45 m
Normalised emittance	2.2 μm

the LHC ones both in units of the beam standard deviation σ and in mm, in order to avoid excessive impedance and to guarantee mechanical stability while keeping the σ-setting small enough to protect the aperture. This is possible, since the limiting aperture bottleneck in the ring at collision in units of beam σ is similar to the LHC, as discussed in Sec. 5.2. The number of collimators and their phase advances are the same as in the LHC and were optimised for three-stage cleaning [20]. Primary collimators (TCP), closest to the beam, intercept primary proton losses and give rise to a secondary halo that is intercepted by secondary collimators (TCS). Active absorbers (TCLA), placed at apertures further out than the TCS, catch showers from upstream collimators.

A similar three-stage cleaning is installed in ESS-J for momentum collimation, with the difference that the horizontal dispersion in ESS-J is much higher than in ESS-D (see Figure 2 bottom), maximising the normalized dispersion near the primary collimators. The dispersion functions of the momentum cleaning insertion are the same as at the LHC. The betatron functions are scaled with a factor $k_p = \sqrt{50/7} = 2.7$, derived from the ratio of the centre-of-mass energies of the FCC-hh to the LHC. This scaling factor is smaller than that used for the betatron cleaning insertion allowing to shorten the length to 1.4 km. Constraints from impedance and mechanical stability are in fact less tight in the momentum cleaning insertion because primary collimators for momentum cleaning can be kept more opened in σ than those for betatron cleaning. The momentum cleaning system is designed to capture losses only in the horizontal plane, while the betatron cleaning system ensures coverage in the whole transverse space.

In addition, tertiary collimators (TCT) are installed in the low-beta insertions, about 220 m upstream the interaction point, to provide local protection of the inner triplets. At the beam extraction, a dump protection collimator

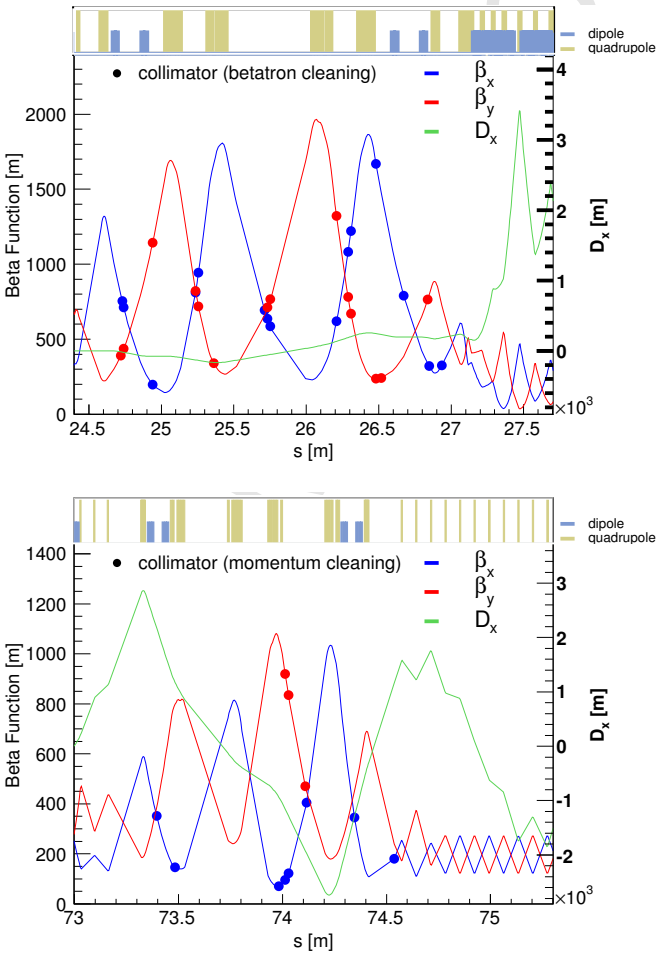

Figure 2: Optical functions for the betatron (top) and momentum (bottom) cleaning insertions. The markers show the location of collimators in the relevant plane (ie. horizontal and vertical collimators are omitted in the vertical and horizontal plane respectively, while skew collimators have a marker in both planes).

(TCDQ) is installed as a protection against miskicked beams in the case of extraction failures. Note that injection protection collimators are not yet part of this layout. Another important functionality of the LHC collimation system that was not yet finalized for FCC-hh is the physics debris collimation downstream of the collision points. These aspects are not relevant at this stage for the assessment of the collimation cleaning performance and will be addressed in the next layout iteration.

In this first iteration, the same collimator jaw materials and lengths as at the LHC are taken as a first design assumption. These are summarised in Table 3. This initial assumption is justified by the fact that only a small fraction of the total energy deposited by the impacting proton is absorbed by the collimators, while the highest fraction goes to passive absorbers and the tunnel walls. An optimisation of the collimator design will be performed in separate studies. It is planned to modify the collimator materials in the future, based on the outcome of new material studies that are ongoing [21] in the context of the high-luminosity upgrade of the LHC, HL-LHC [22, 23]. Further improvements of the system, such as addition of more collimators and optimisation of phase advances will also be studied.

Table 3: Collimator jaw material and length and baseline collimator settings at injection (3.3 TeV) and collision (50 TeV) energy, expressed in units of betatron σ for a normalised emittance of 2.2 μm and the nominal β-functions.

Description	**Name**	**Length [m]**	**Material**	**Settings [σ]**	
				Injection (3.3 TeV)	**Collision (50 TeV)**
Betatron cleaning	TCP	0.6	C	7.2	7.2
	TCS	1.0	C	9.7	9.7
	TCLA	1.0	W	12.0	12.0
Momentum cleaning	TCP	0.6	C	11.0	21.4
	TCS	1.0	C	12.6	25.2
	TCLA	1.0	W	16.0	27.7
Extraction	TCDQ	9.0	C	11.4	11.4
Tertiaries	TCT	1.0	W	30	13.7

4. Baseline collimator settings

Collimator settings have to be defined in a way that ensures protection of the minimum machine aperture with sufficient margin. Furthermore, a strict hierarchy between collimator families must be respected for optimal cleaning performance and machine protection.

By design at collision energy the aperture limitation typically lies in or close to the inner triplet, since at this location the available aperture is reduced by the large β-functions required to achieve small beam sizes at the interaction points and by the crossing and separation schemes. This constrains the opening

of the tertiary collimators (TCT). In the present LHC system, TCTs are not robust against direct beam losses and thus have to be placed outside protection devices, such as the TCDQ, which in turn should be at larger aperture than TCPs and TCSs [10, 24]. For FCC-hh, we define settings in a similar way to minimise the risk of major losses close to the experiments.

At injection energy the aperture bottleneck is instead in the arcs, which has to be protected by the betatron and momentum cleaning systems, while the TCTs can be more open.

The limitations of the arc aperture, which is minimized to optimize the cost of the superconducting dipoles and quadrupoles, are discussed in more details below. They translate into similar constraints on the betatron collimation hierarchy as the ones encountered at top energy.

In Table 3 we present the baseline collimator settings for the FCC-hh at injection and collision energy that provide a minimum protected aperture of 15.5 σ. The settings for betatron cleaning, extraction and tertiary collimators correspond to the HL-LHC baseline settings [25] scaled to the FCC-hh normalised emittance of 2.2 μm and result in collimator gaps (in mm) that are comparable to the LHC ones.

The settings for momentum cleaning collimators are defined such that they provide a cut in momentum $\delta p/p$ (where p is the particle momentum) that is tighter than the momentum acceptance of the machine. At injection, the tightest off-momentum aperture bottlenecks typically occur in the arcs, at locations with peak horizontal dispersion function, D_x. Furthermore, the collimation hierarchy in the betatron cleaning insertion must not be violated, implying that the opening of momentum cleaning collimators expressed in units of beam σ should be larger than the TCPs and TCSs of the betatron cleaning insertion. The FCC-hh arc acceptance is:

$$\left(\frac{\Delta p}{p}\right)^{\mathrm{arc}} = \frac{A^{\mathrm{arc}}}{D_x^{\mathrm{arc}}} = 0.71\%, \tag{5}$$

where A^{arc} is the aperture in the arc and D_x^{arc} is the maximum dispersion in the arc. Considering the above constraints, the TCPs of the momentum cleaning insertion were chosen to provide a momentum cut of 0.24% at injection energy and 0.12% at collision energy.

Detailed aperture studies that take into account optical and mechanical tolerances are necessary to validate and, if necessary update, the settings at injection and collision energy. This is the topic of the next section.

5. Geometrical acceptance of the machine

5.1. Method and input parameters

A first continuous aperture model for the whole FCC-hh ring was defined. The geometrical aperture of the arc is given by the beam screen, assumed to be of so-called "rect-ellipse" shape similar to the one adopted for the LHC, defined by the intersection of an ellipse and a rectangular aperture. The dimensions

are 2×15 mm (width) and 2×13.2 mm (height). In the collimation insertion and matching sections, the same mechanical aperture in mm as in the LHC was assumed. The mechanical aperture in the experimental insertion was designed as described in [26]. The effective aperture of the machine was then computed element by element using the aperture module of the MADX code [27, 28, 29, 30]. This calculation finds the minimum clearance in 2D, in units of beam σ, between the closed orbit and the mechanical aperture. The calculation is repeated for several longitudinal positions within every magnet. A number of tolerances are included to account for imperfect optics and orbit (see in Table 4). This parameter set, proposed in [25] to calculate the HL-LHC aperture, was refined with respect to the LHC design parameters based on operational experience. As there are still many unknowns in the FCC design, we assume at this stage that the state-of-the-art correction assumed for HL-LHC can be reached also in FCC-hh. In the future, when the machine design is more final, these tolerances should be refined. In addition, the same mechanical and alignment tolerances as for the present LHC [31] were assumed conservatively for a first aperture assessment. Aperture parameters and mechanical tolerances used for each magnet class are detailed in Appendix B.

Table 4: Optical tolerances for aperture calculations at injection and collision energy.

Parameter	**Name**	**Injection**	**Collision**
Radial closed orbit excursion	CO^{peak}	4 mm	2 mm
Beta-beating	$\Delta\beta/\beta$	10%	21%
Momentum offset	δ_p	6×10^{-4}	2×10^{-4}
Relative parasitic dispersion	k_D	0.14	0.10

5.2. Aperture at injection and collision energy

Aperture studies were performed for the layout and optics presented in Sec. 3. The effective aperture, expressed in units of σ (where σ is the local betatron beam size computed using a normalised emittance of 2.2 μm), was compared to the specifications of 15.5 σ, the minimum aperture that is protected using the collimator settings of Table 3. Results at injection and collision energy are shown in Figures 3 and 4, respectively. Table 5 presents the aperture in IPG, the experimental IR, at both injection and collision energy.

At injection energy, an aperture below the specifications was found in several sections of the machine. In the arc cells, in particular, the minimum aperture is 13.4 σ in the sextupoles next to the focusing quadrupoles. Small apertures were also found in the cleaning insertions, the minimum aperture being below 10 σ in an trim quadrupole of the betatron cleaning insertion. This can be explained by the large β-functions, which were scaled by a factor $k = 5$ from the LHC, while the magnet apertures remained the same as at the LHC. The warm magnet design will have to be reviewed to take this into account. A revision of the collimator setting hierarchy at injection and of the assumed tolerances and imperfections is planned to solve the problem of arc aperture.

At collision energy, the aperture bottleneck of the ring was found in the low β insertions, at the location of the recombination dipole D2 with a value of 14.1 σ. The available aperture is in fact reduced by the large β-functions required to achieve small beam sizes at the interaction points and by the crossing and separation schemes. However the exact location of the aperture bottleneck in the IR depends on the design of the experimental insertion. While in the previous experimental IR design, with the inner triplet layout characterised by $L^\star = 36$ m, the aperture bottleneck was in the inner triplet [32], in the current one with $L^\star = 45$ the inner triplet aperture is above 40 σ and the bottleneck is shifted to the recombination dipole D2. In the present collimation layout, tertiary collimators are placed to provide local protection of the inner triplet, like in the LHC where this is the aperture bottleneck.

The IR design of the FCC-hh is still being revised and if additional shielding is added to the inner triplet effectively reducing the available aperture as proposed in [33], the triplet is likely to become the aperture bottleneck as in the LHC. If instead D2 remains the bottleneck, the location of tertiary collimators should be reviewed in the future to provide local protection of D2 as well. A similar approach is being followed for the IR design at the HL-LHC, where a second pair of TCT collimators will be added further upstream of the TCTs that protect the triplet. These new collimators will protect other magnets in the matching section whose aperture is reduced for various optics scenarios with very small $\beta^\star$ [22, 23].

Table 5: Geometrical acceptance in units of beam σ in the low-β insertion IPG at injection and collision energy. For each elements right and left of the IP, only the smallest aperture value is reported.

Element	**aperture** [σ]	
	Injection	Collision
Triplet magnet, IP side (Q1)	53.0	52.0
Triplet magnet, central (Q2)	42.6	41.4
Triplet magnet, non-IP side (Q3)	43.1	41.9
Recombination dipole, IP side (D1)	17.5	17.7
Recombination dipole, non-IP side (D2)	12.5	14.1

5.3. Conclusion of aperture studies

The aperture limitations identified by these first aperture studies can be fed back to revise the aperture model (physical aperture of the magnets) or the magnet mechanical tolerances. With this goal, for each element of the machine, the margin left to reach the specifications of 15.5 σ was computed in mm for the horizontal and vertical planes. Table 6 shows these values for elements with aperture below the specifications at injection energy. For each magnet class, the limiting plane is indicated and the value in mm shows by how much the physical aperture or the mechanical tolerances should be improved. In some cases, as for the arc, if the aperture cannot be improved, the collimator settings should

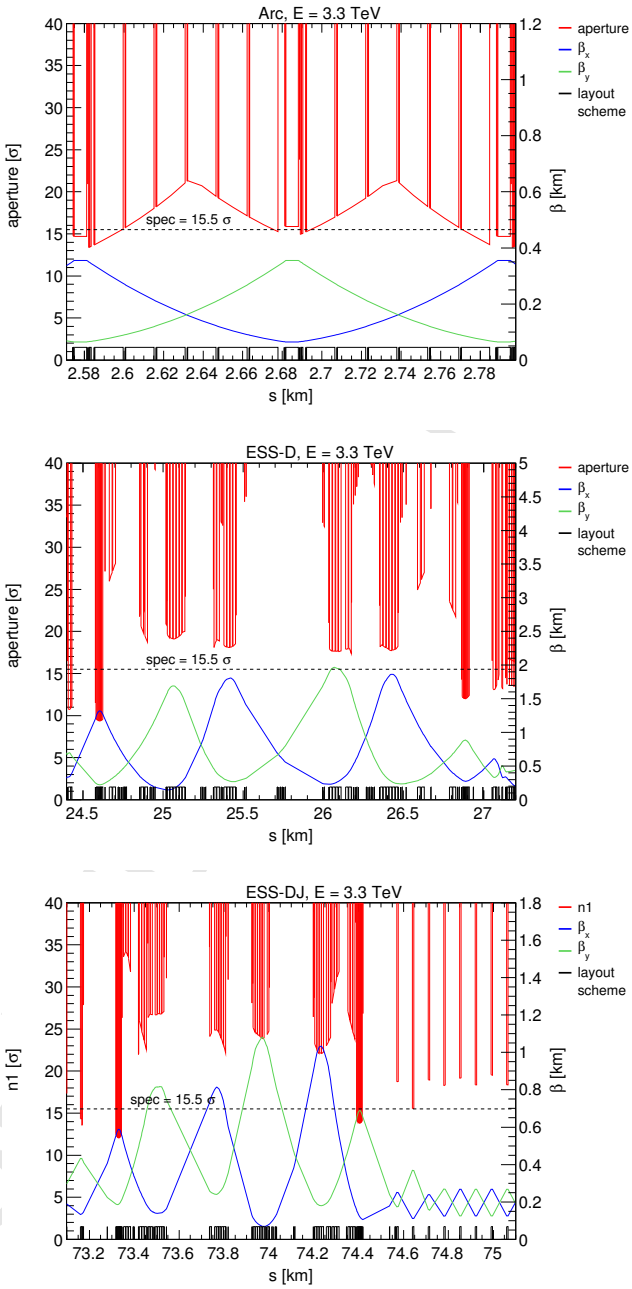

Figure 3: Geometrical aperture in units of beam σ at the injection energy of 3.3 TeV in the FCC-hh cell (top), in the betatron cleaning insertion ESS-D (middle) and in the momentum cleaning insertion ESS-J (bottom). The dotted line shows the target minimum protected aperture of 15.5 σ.

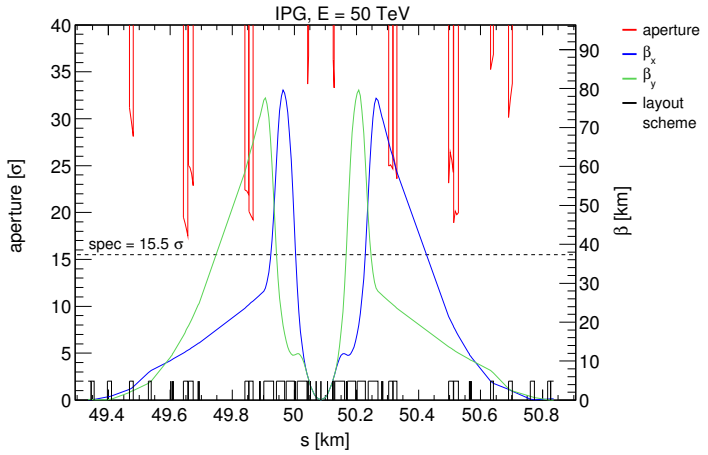

Figure 4: Geometrical aperture in units of beam σ at the collision energy of 50 TeV in the interaction point IPG. The dotted line shows the target minimum protected aperture of 15.5 σ.

be revised and made compatible with a smaller protected aperture. An overall improvement of the assumed tolerances, compared to what was assumed in the LHC design phase, is also not to be excluded.

While more studies and iterations are needed to finalize the detailed aperture designs for FCC, as well as possible refinements of the error tolerances and acceptance criterion for the aperture, we consider that this status is adequate as first input to the collimation design that is presented in the next section.

Table 6: List of elements with aperture below the specification of 15.5 σ at injection energy. For each element, the plane with limiting aperture is indicated and the required aperture improvement in mm is calculated. For each magnet class, only the element with the minimum aperture value is reported.

Element class	**Aperture [σ]**	**Plane**	**Margin [mm]**
Main dipole	13.5	H	-0.6
Main quadrupole	12.0	H	-1.6
IR matching quadrupoles	13.5	H	-0.7
IR separation dipoles	12.5	H (V)	-2.6
Dump region quadrupole	10.9	H	-7.8
Betatron collimation matching quadrupole	9.4	H	-5.1
Momentum collimation matching quadrupole	12.1	H	-1.7

6. Simulations of collimation cleaning performance

6.1. Tracking simulations

Tracking simulations were performed with SixTrack [34, 35, 36, 37, 38] to assess the cleaning performance. In these simulations, the processes that cause protons to diffuse out to high betatron amplitudes are not included. Instead, in order to have a simulation setup that is feasible in terms of computing time, the starting conditions are sampled such that the protons impact on the primary collimators during the first few turns. The initial particle distribution was a direct halo [38] at 7.2 σ and a thickness $\delta\sigma = 0.06$ in the horizontal plane, a normal distribution cut at 3 σ in the vertical plane and no energy errors. The average impact parameter b on the TCP was about 16 μm and 4 μm at injection and collision energy, respectively. Since the diffusion speed of halo protons at the FCC-hh is hard to assess at this stage, a range of different impact parameters b (between 1 μm and 12 μm) on the primary collimator were simulated in order to assess the effect of the assumed initial distribution. The cleaning inefficiency was found to change by about 20% between the extreme values of b. Large statistics is needed to reach a precision level for loss spikes which is below the assumed quench levels. Therefore, for the simulations presented here, 8.9 million particles were tracked for 200 turns for the case of a perfect machine and using collimator settings from Table 3.

The SixTrack simulation performs a 6D element-by-element tracking through the magnetic lattice and if a proton interacts with a collimator, a built-in scattering model is used. If an inelastic interaction occurs, in which the proton disintegrates, it is considered lost on the collimator and removed from the tracking. Otherwise, it can scatter out again and the tracking continues. If a proton hits with the aperture of any other element, such as cold magnets, it is considered lost there without further study of the shower development. The output of the tracking simulations is both η_c, estimated from the distribution of surviving halo particles at a fixed longitudinal position downstream of the collimation system, as well as the distribution of lost protons around the ring, from which the local cleaning efficiency $\tilde{\eta}_c$ can be determined.

6.2. Cleaning inefficiency

A first assessment of the collimation system performance can be made by studying the cleaning inefficiency η_c, as explained in Sec. 2. η_c has the advantage of being independent of the longitudinal coordinate s and can be studied without an aperture model. Eq. (1) defines η_c as a function of the radial amplitude A_0.

Similarly, to study the off-momentum halo population escaping the collimation system, we can define a cleaning inefficiency as a function of the relative momentum deviation $\delta p/p$, by substituting into Eq. (1) the amplitude A_0 with $\delta p/p$. These functions are computed from tracking simulations by assessing, in the multi-turn simulation setup, the number of particles that populate the halos as a function of their transverse radial amplitude and of their energy offsets, respectively.

The cleaning inefficiency of the system at collision energy is shown in Fig. 5. At an aperture of 15.5 σ, corresponding to the minimum protected aperture for the baseline collimator settings, the cleaning inefficiency is below 10^{-4}, while above $\delta p/p = 0.4\%$ the cleaning inefficiency is below 10^{-6} (for reference, the momentum acceptance of the arc $\delta p/p = 0.7\%$).

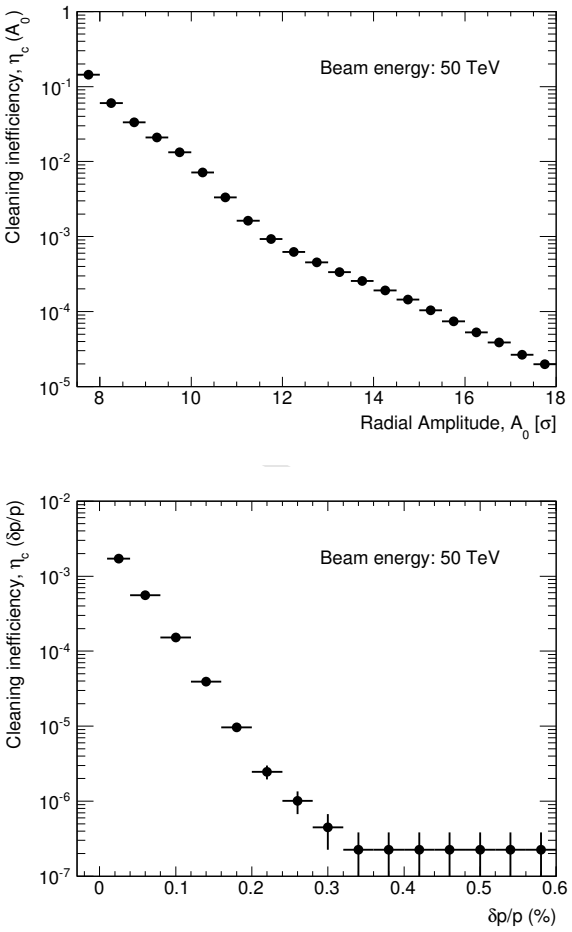

Figure 5: Cleaning inefficiency as a function of radial amplitude A_0 (top) and momentum off-set $\delta p/p$ (bottom) at collision energy. The horizontal error bars represent the bin width, while the vertical ones are the statistical errors on the efficiency and are calculated as $\sqrt{\eta_c(1-\eta_c)/N_{abs}}$, where η_c and N_{abs} are defined in Eq. 1.

The cleaning inefficiency can already be used to optimize the system performance, in absence of a machine aperture module. Figure 6 displays the cleaning inefficiency $\eta_c(A_0)$ as a function of the settings of the betratron cleaning secondary collimators, at different values of radial amplitude A_0. This example

illustrates how the settings of the secondary collimators can be optimized and ensure that the cleaning performance meets the specifications.

For example, by looking at the curve for $A_0 = 10\ \sigma$, it can be seen seen that the settings of the TCS at 9.7 σ derived from the present LHC operational settings, are not at an optimum. An improvement could be obtained by tightening the settings, at the expense of the machine impedance and operational tolerance. This is not a change that can be proposed at this stage. It is instead planned to re-optimize the betraton phases between TCS and TCP as a possible improvement.

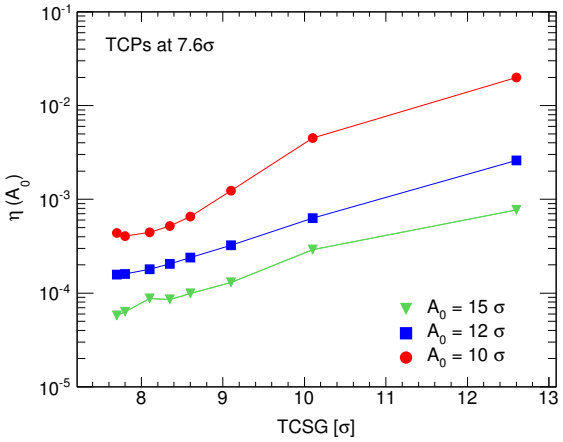

Figure 6: Cleaning inefficiency $\eta_c(A_0)$ as a function of the settings of secondary collimators. Only betatron cleaning was considered for this study. TCPs were set at 7.6 σ. The different curves show the cleaning inefficiency sampled at different values of A_0.

6.3. Loss maps at injection and collision energy

Loss maps allow to study in details the local cleaning inefficiency $\tilde{\eta}_c$, that is how particles escaping the collimation system are lost longitudinally around the ring. This allows a direct comparison to magnets' quench limits. Horizontal loss maps are shown in Figure 7 and Figure 8 for injection and collision energy, respectively, with a resolution of 10 cm in s. A zoom is shown in locations with large losses: the betatron and the momentum cleaning insertions and one of the two interaction points.

The most significant cold losses occur at $s \sim 27.2$ - 27.5 km in the dispersion suppressor (DS) immediately downstream of the cleaning insertion, where two clusters of losses are observed in correspondence to local peaks in the dispersion function. The peak $\tilde{\eta}_c$ is reached in the second cluster of ESS-D with a value of $(1.1 \pm 0.4) \times 10^{-5}$ m^{-1} and $(3.7 \pm 0.6) \times 10^{-5}$ m^{-1}, at injection and collision energy, respectively. At collision energy, this value is about two orders of magnitude above the assumed quench level of 3×10^{-7}m^{-1}. It is clear that these

losses are not acceptable for the performance requirements of the FCC-hh. A detailed analysis of these losses and possible solutions will be discussed in the next section.

Other important losses occur around the interaction points (IPs) in correspondence with aperture restrictions at the location of the recombination dipoles. At injection energy, these losses are higher than those in the DS regions downstream of ESS-D. If the magnet aperture cannot be increased, these losses can be cured by carefully positioning tertiary collimators for local protection of the dipole magnets.

At collision energy, losses at the level of 6×10^{-6} are also observed in the dispersion suppression region after the IPs, in correspondence to local peaks in the dispersion function. Such losses are not observed at injection energy: tertiary collimators are in fact retracted and protons are intercepted earlier by the aperture restriction in correspondence of the recombination dipole. As shown below, these losses are mitigated by the proposed solutions for the losses in the DS downstream of the collimation insertion.

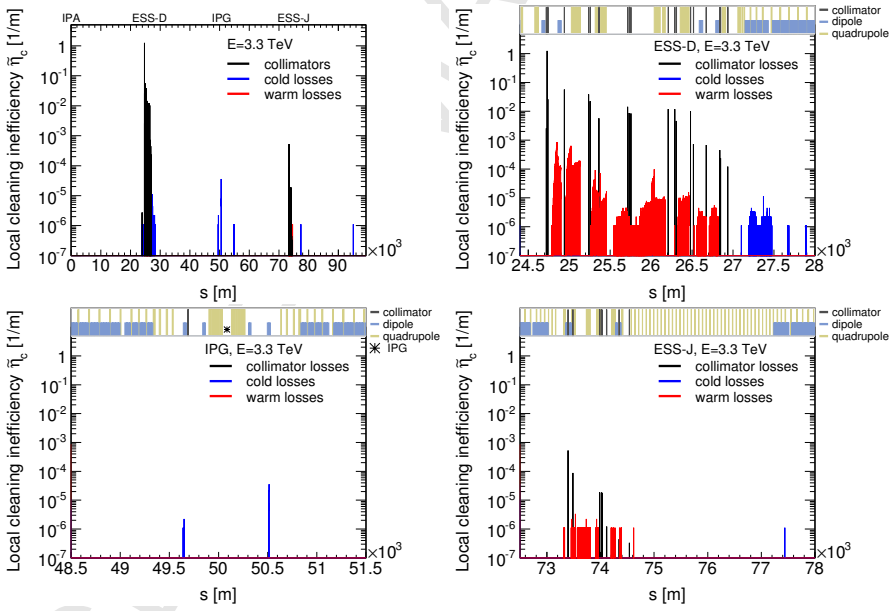

Figure 7: Horizontal loss map at injection energy of 3.3 TeV for the entire ring (top left), zoom in the betatron cleaning insertion ESS-D (top right), in the interaction point G (bottom left) and in the momentum cleaning insertion ESS-J (bottom right). The interaction points A and G are located at $s = 0$ and 50×10^3 m respectively, while ESS-D and ESS-J start at about $s = 23 \times 10^3$ and 73×10^3 m respectively. The dispersion suppressors at end of the cleaning insertions are located at about $s = 27.1 - 27.6 \times 10^3$ and $77.2 - 77.8 \times 10^3$ m.

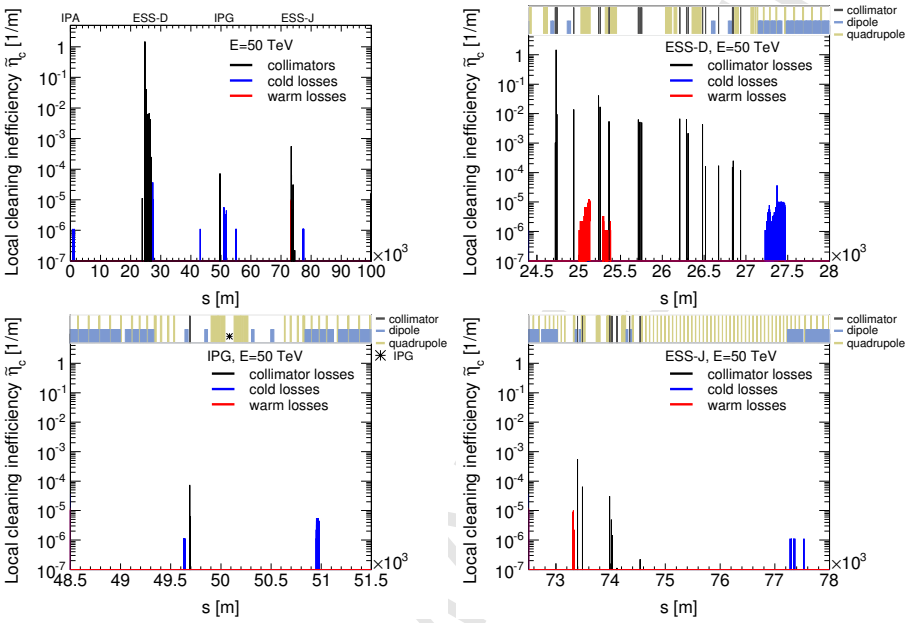

Figure 8: Horizontal loss map at collision energy of 50 TeV for the entire ring (top left), zoom in the betatron cleaning insertion ESS-D (top right), in the interaction point G (bottom left) and in the momentum cleaning insertion ESS-J (bottom right). The interaction points A and G are located at $s = 0$ and 50×10^3 m respectively, while ESS-D and ESS-J start at about $s = 23 \times 10^3$ and 73×10^3 m respectively. The dispersion suppressors at end of the cleaning insertions are located at about $s = 27.1 - 27.6 \times 10^3$ and $77.2 - 77.8 \times 10^3$ m.

7. Optimisation of the betatron cleaning insertion

As shown in Section 6.3, the performance of the current system is limited by the losses in the DS downstream of the betatron cleaning insertion. These losses are due to protons that survive the passage through the TCPs but have lost energy in single diffractive interactions. As their kick in betatron amplitude is small, they do not hit the downstream TCSG in the straight section, but when the dispersion starts to rise in the first dipoles in the DS, they are bent differently than the main beam and soon lost on the aperture. The distribution of δp/p of particles escaping the collimation insertion and lost around the FCC-hh ring is shown in Figure 9. Particles lost in the DS have a characteristic distribution with $\delta \mathrm{p/p} < -5 \cdot 10^{-3}$.

Similar performance limitations are observed at the LHC and have been extensively studied in the context of the HL-LHC upgrade [39]. The HL-LHC solution consists in the installation of new collimators in the DS upstream of the critical locations, but where there single-pass dispersion from the TCPs is already rising. This solution intercepts locally parts of the beam halo with a significant off-momentum component and has also the advantage to reduce losses in other locations around the ring.

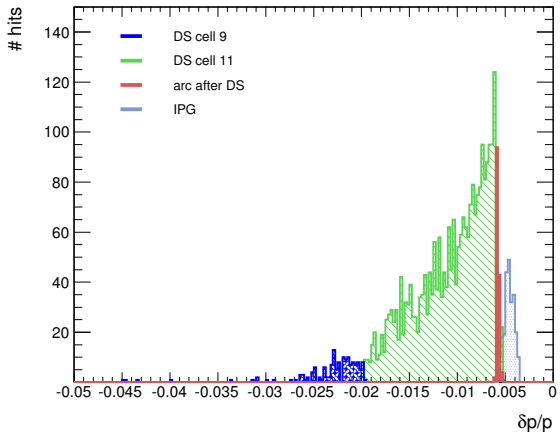

Figure 9: $\delta p/p$ distribution of particles lost around the ring, after the betatron cleaning insertion: in the first and in the second cluster of the DS after ESS-D (DS cells 9 and 11), in the arc after the DS and in IPG.

In this section an analogous solution for the FCC-hh is investigated. The performance of the system with the addition of local protection collimators in the DS, which we call TCLD collimators, is investigated with a reduced collimation layout with respect to that presented in Sec. 3, and including only the betatron cleaning insertion and tertiary collimators.

For the LHC, TCLD collimators can only be installed in the DS by replacing the existing dipole magnets with shorter, higher field dipoles that free space to install a collimator at room temperature. This is a cumbersome intervention. Obviously, for FCC-hh the installation of TCLD collimators must be planned early on in the design of the dispersion suppressors. The optics function at the proposed locations for the TCLD collimators are summarized in Table 7. The proposed layout is shown in Figure 10.

Table 7: Optical functions at the proposed locations of the TCLD collimators, collimator settings and resulting δp/p cut and half-gap.

Collimator	β_x [m]	β_y [m]	D_x [m]	Setting [σ]	δp/p cut	Half-gap [mm]
TCLD.8RD	72	164	0.10	24	1.3×10^{-2}	1.31
TCLD.10RD	54	447	0.69	24	1.7×10^{-3}	1.13

Figure 11 shows the betraton loss maps simulated around the full ring (top graph) and in the collimation insertion (bottom) for the new layout of Figure 10 with two TCLD collimators installed in the cells 8 and 10 of the DS. These collimators are very efficient in catching the dispersive losses. The number

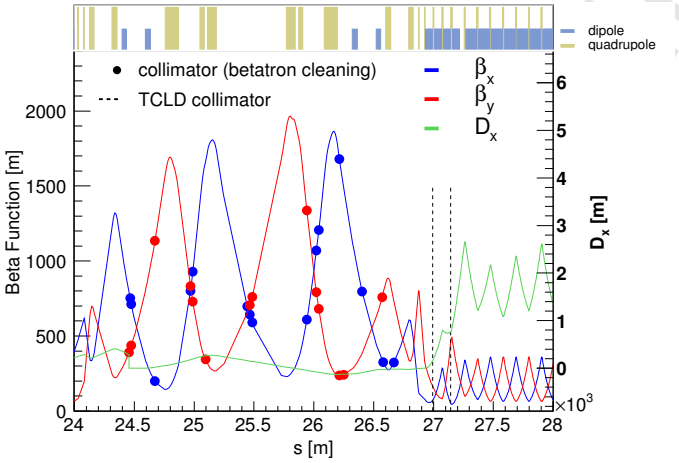

Figure 10: Optics functions of the betatron cleaning insertion with the proposed locations for the TCLD collimators, called TCLD.8RD and TCLD.10RD. The markers show the location of collimators in the relevant plane (ie. horizontal and vertical collimators are omitted in the vertical and horizontal plane respectively, while skew collimators have a marker in both planes).

of protons reaching the aperture of DS magnets is now reduced to less than a few 10^{-7}/m. In addition, cold losses around the ring are also significantly suppressed. This is expected since the momentum cuts provided by the TCLD collimators, as listed in Table 7, are smaller than the typical energy errors of the halo particles escaping ESS-D (Figure 9). While a final performance assessment of this collimation layouts with TCLD will have to be carried out after having computed the detailed energy deposition maps in critical elements, these results indicate that the proposed solution has the potential to deliver adequate halo cleaning performance for the design FCC-hh parameters.

8. Conclusions and outlook

In the context of the FCC-hh study, a first conceptual solution of a halo collimation system for a 50 TeV proton accelerator has been worked out. The ambitious FCC-hh goal to accumulate stored beam energies up to 8.5 GJ, which surpasses by more than a factor 20 the present state-of-the-art set by the operating Large Hadron Collider, poses outstanding concerns for the operation in a superconducting environment. A collimation cleaning performance well below the 10^{-6} level is expected to be needed to operate reliably such an accelerator below quench limits of superconducting magnets.

As a starting point for the studies, we have shown first estimates of the available machine aperture for FCC-hh. Although many elements have a sufficient beam-stay-clear, there are a few points of concern that need further studies

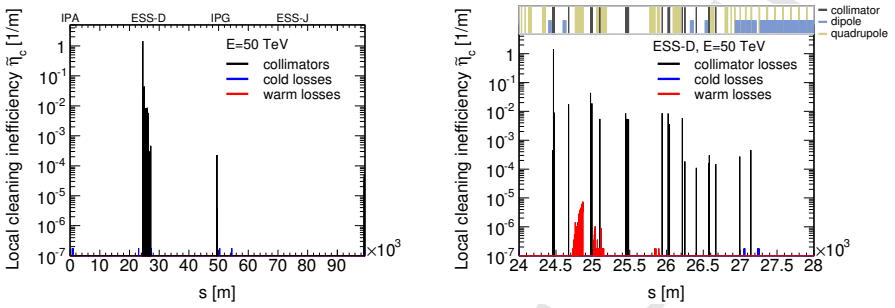

Figure 11: Horizontal loss map for the entire ring (top) and zoom in the betatron cleaning insertion ESS-D (bottom) with two TCLD collimators, one in cell 8 and one in cell 10.

and optimization to meet the requirements, in particular the arc dipoles, the warm dipoles in the collimation insertions and the separation dipoles around the experiments.

We have shown a first design of a collimation system for the FCC-hh, derived from the present LHC system, which has a proven successful performance with stored beam energies up to 300 MJ. The operational experience obtained with the LHC system, as well as the results of the new studies carried out in recent years for the HL-LHC upgrade, have been built into the FCC-hh collimation design. It features, at this early stage, a complete layout with two separate multi-stage betatron and off-momentum cleaning insertions, tertiary collimators in the experimental regions and special protection devices in the dump protection region. This system is almost complete and certainly adequate for a first reliable assessment of cleaning performance at the FCC-hh. Injection protection collimators and physics debris cleaning systems were not yet integrated but this is not considered critical for the assessment of the cleaning performance that drives the key design features for the FCC-hh.

With the addition of dispersion suppressor collimators around the betatron cleaning insertion, the proposed FCC-hh system provides cleaning inefficiencies of a few units of 10^{-7} proton per meter lost in superconducting magnets per proton impinging on the primary collimators. This is a very encouraging starting point that however must be confirmed by more complete studies that include energy deposition assessment for the most exposed components. The tools shown in this paper are ready to provide the required inputs for these studies, which have in fact already started. This effort will also address the compatibility of the present LHC collimator design, assumed as a starting point, with the challenging beam loads expected from FCC-hh beam losses. Preliminary results indicate that this is indeed an important concern for a few selected collimators which might require a substantial re-design [11]. Furthermore, it also has to be studied how the cleaning performance evolves in the presence of realistic imperfections in the collimation system and in the optics.

At this stage, we consider this scaled-up scheme a promising first design of

a collimation system in preparation of a conceptual design of FCC-hh, although there are still a few open points to be addressed. This conservative design approach will be extended with more advanced collimation concepts. However, at this stage, this conceptual solution already provides a very promising performance for halo cleaning, which on paper is close to the FCC-hh design goal.

Acknowledgments

The authors would like to acknowledge the members of the LHC collimation team in the CERN Accelerator Physics Group, in particular D. Mirarchi, and collaborators from the FCC-hh teams: A. Chance, B. Dalena, A. Faus-Golfe, B. Holzer, R. Martin, J. Molson, D. Schulte. We would also like to thank the optics team that provided the optics for the collimation cleaning insertion (R. Tomas, A. Langner, X. Buffat).

Appendix A. Overview of collimators in the FCC-hh baseline layout

A complete list of collimators included in the FCC-hh baseline layout is given in Table A.8. The full name of each device is shown, as well as the optics and settings.

Appendix B. FCC-hh aperture model

Table B.9 shows an overview of the different magnet classes used for the FCC-hh aperture calculations. The equipment class names are presented, along with a short description of each category. In Table B.10 we show the dimensions of the vacuum chamber for each class, as well as the assumed transverse mechanical tolerances in the horizontal, vertical and radial (along the 45° line) directions. Since the FCC-hh magnet design is not yet progressed to a stage where these tolerances can be predicted reliably, we assume the same mechanical tolerances as for the present LHC machine [40]. They include tolerances for cryostat assembly, dynamic movements, survey error and tunnel movements.

References

[1] Web page of the fcc design study.
URL `https://fcc.web.cern.ch/Pages/default.aspx`

[2] R. Tomas, et al., FCC study: parameters and optics for hadron and lepton colliders, Nucl. Part. Phys. Proc. 273-275 (2016) 149–155. 7 p.

[3] O. Brüning, P. Collier, P. Lebrun, S. Myers, R. Ostojic, J. Poole, P. Proudlock, LHC Design Report, CERN Yellow Reports: Monographs, CERN, Geneva, 2004.

[4] L. Burnod, J. B. Jeanneret, Beam losses and collimation in the LHC: a quantitative approach, Tech. Rep. CERN-SL-91-39-EA. LHC-NOTE-167. CERN-LHC-Note-167, CERN (1991).

[5] T. Trenkler, J. B. Jeanneret, The Principles of the Two-stage Betatron and Momentum Collimation in Circular Accelerators, Tech. Rep. CERN-SL-95-03-AP. LHC-NOTE-312., CERN (1995).

[6] M. A. Maslov, N. V. Mokhov, I. A. Yazynin, The SSC Beam Scraper System, Tech. Rep. SSCL-848, SSC (1991).

[7] J. M. Butler, et al., Reduction of Tevatron and Main Ring Induced Backgrounds in the D0 Detector, Fermilab-FN-629 (1995).

[8] M. Seidel, The Proton Collimation System of HERA, DESY 94-103 (1994).

[9] D. Mirarchi, et al., Collimation: experience and performance, Proceedings of the 7th Evian Workshop on LHC beam operation, Evian, France (2016).

[10] R. Bruce, C. Bracco, R. D. Maria, M. Giovannozzi, A. Mereghetti, D. Mirarchi, S. Redaelli, E. Quaranta, B. Salvachua, Reaching record-low β^* at the CERN Large Hadron Collider using a novel scheme of collimator settings and optics, Nucl. Instr. Meth. Phys. Res. A 848 (2017) 19 – 30. doi:http://dx.doi.org/10.1016/j.nima.2016.12.039.
URL //www.sciencedirect.com/science/article/pii/S0168900216313092

[11] M. I. Besana, et al., Energy Deposition in the Betatron Collimation Insertion of the 100 TeV Future Circular Collider, in: Proc. of International Particle Accelerator Conference (IPAC'17), Copenhagen, Denmark, 2017, p. 68.

[12] R. Assmann, Collimators and cleaning: could this limit the LHC performance?, Proceedings of the LHC Performance Workshop: Chamonix XII, Chamonix, France (2003).

[13] G. Robert-Demolaize, Design and performance optimization of the LHC collimation system, Ph.D. thesis, Universite Joseph Fourier, Grenoble (2006).
URL http://cds.cern.ch/record/1004869

[14] C. Bracco, Commissioning scenarios and tests for the LHC collimation system, Ph.D. thesis, EPFL Lausanne (2008).
URL http://cds.cern.ch/record/1174254

[15] D. Schulte, FCC-hh machine layout and optics, presentation at the FCC Week meeting, 2016.04.11.
URL https://indico.cern.ch/event/438866/contributions/1085167

[16] J. B. Jeanneret, et al., Quench levels and transient beam losses in LHC magnets, LHC Project Report 44, CERN (1996).

[17] A. Chance, et al., Status of the beam optics of the Future Hadron-Hadron Collider FCC-hh, in: Proc. of International Particle Accelerator Conference (IPAC'16), Busan, Korea, 2016.

[18] D. Schulte, et al., Collider baseline parameters: Milestone 1.5, CERN-ACC-2016-0082, CERN (2016).

[19] A. Chance, et al., Status of the beam optics of the future hadron-hadron collider FCC-hh, in: Proc. of International Particle Accelerator Conference (IPAC'16), Busan, Korea, 2016, p. 1470.

[20] J. B. Jeanneret, Optics of a two-stage collimation system, Phys. Rev. Spec. Top. Accel. Beams 1 (LHC-Project-Report-243) (1998) 081001. 13 p.

[21] E. Quaranta, et al., Towards Optimum Material Choices for the HL-LHC Collimator Upgrade, in: Proc. of International Particle Accelerator Conference (IPAC'16), Busan, Korea, 2016, p. 2498.

[22] G. Apollinari, I. B. Alonso, O. Brüning, M. Lamont, L. Rossi (editors), High-Luminosity Large Hadron Collider (HL-LHC): Preliminary Design Report, CERN-2015-005 (2015).

[23] G. Apollinari, I. B. Alonso, O. Brüning, P. Fessia, M. Lamont, L. Rossi, L. Tavian (editors), High-Luminosity Large Hadron Collider (HL-LHC) : Technical Design Report V. 0.1, CERN-2017-007-M (2017).

[24] R. Bruce, R. W. Assmann, S. Redaelli, Calculations of safe collimator settings and β^* at the CERN Large Hadron Collider, Phys. Rev. ST Accel. Beams 18 (2015) 061001. doi:10.1103/PhysRevSTAB.18.061001.
URL http://link.aps.org/doi/10.1103/PhysRevSTAB.18.061001

[25] R. Bruce, et al., Parameters for HL-LHC aperture calculations and comparison with aperture measurements, Tech. Rep. CERN-ACC-2014-0044, CERN, Geneva (2014).

[26] R. Martin, R. Tomas, Interaction region for a 100 TeV proton-proton collider, in: 6th International Particle Accelerator Conference (IPAC' 2015), Richmond, VA, USA, 2015, p. 1996.

[27] MAD-X program.
URL http://madx.web.cern.ch/madx/

[28] H. Burkhardt, et al., Upgrade of slicing and tracking in MAD-X, in: Proc. of International Particle Accelerator Conference (IPAC' 2014), Dresden, Germany, 2014.

[29] J. Jeanneret, T. Risselada, Geometrical aperture in LHC at injection, LHC Project Note 66, CERN (1996).

[30] J. Jeanneret, R. Ostojic, Geometrical acceptance in LHC version 5.0, LHC Project Note 111, CERN (1997).

[31] J. B. Jeanneret, R. Ostokic, Geometrical Acceptance in LHC Version 5.0, Tech. Rep. LHC-Project-Note-111, CERN, Geneva (1997).

[32] M. Fiascaris, et al., First design of a proton collimation system for 50 TeV FCC-hh, in: Proc. of International Particle Accelerator Conference (IPAC'16), Busan, Korea, 2016, p. 2423.

[33] M. I. Besana, Shielding of triplet from collision debris, in: EuroCirCol meeting, ALBA Synchrotron, Barcelona, Spain, 2016.
URL https://indico.cern.ch/event/563053/

[34] Sixtrack.
URL http://sixtrack.web.cern.ch/SixTrack/

[35] F. Schmidt, SIXTRACK version 1.2: single particle tracking code treating transverse motion with synchrotron oscillations in a symplectic manner; user's reference manual, Tech. Rep. CERN-SL-94-56-AP, CERN (1994).

[36] E. McIntosh, R. De Maria, The SixDesk Run Environment for SixTrack, Tech. Rep. CERN-ATS-Note-2012-089 TECH, CERN (2012).

[37] G. Robert-Demolaize, et al., A New Version of SixTrack with Collimation and Aperture Interface, in: Proc. of the Particle Accelerator Conference (PAC 2005), Knoxville, Tennessee, US, 2005, p. 4084.

[38] R. Bruce, et al., Simulations and measurements of beam loss patterns at the CERN Large Hadron Collider, Phys. Rev. ST Accel. Beams 17 (2014) 081004. doi:10.1103/PhysRevSTAB.17.081004.
URL http://link.aps.org/doi/10.1103/PhysRevSTAB.17.081004

[39] R. Bruce, et al., Cleaning performance with 11T dipoles and local dispersion suppressor collimation at the LHC, in: Proc. of International Particle Accelerator Conference (IPAC' 2014), Dresden, Germany, 2014, p. 170.

[40] J. B. Jeanneret, Geometrical tolerances for the qualification of the LHC magnets, Tech. Rep. LHC-PROJECT-Report-1007, CERN, Geneva (2006).

Table A.8: List of collimators included in the baseline. For each collimator, the azimuthal orientation of the jaws, the optical functions, the settings in beam σ and the half-gap (in mm) at top energy are indicated. The collimator names include the family name (TCP/TCS/TCLa/TCT/TCDQ), followed by the cell number and the location (L=left, R=right) with respect to the IP.

Collimator	Azimuth [°]	β_x [m]	β_y [m]	D_x [m]	Setting [σ]	Half-gap [mm]
Dump protection						
TCDQA.A4RD	0.0	2713.2	2716.8	-3.42	11.4	3.82
Betatron cleaning						
TCP.D6LD	90.0	795.6	390.8	-0.01	7.2	0.91
TCP.C6LD	0.0	753.9	413.3	-0.02	7.2	1.27
TCP.B6LD	126.9	713.5	436.9	-0.02	7.2	1.07
TCSG.A6LD	141.1	197.0	1144.2	-0.08	9.7	1.49
TCSG.B5LD	143.5	812.2	822.0	-0.13	9.7	1.78
TCSG.A5LD	40.7	943.1	719.8	-0.13	9.7	1.82
TCSG.D4LD	90.0	1672.0	340.7	-0.16	9.7	1.15
TCSG.B4LD	0.0	692.7	659.7	-0.06	9.7	1.64
TCSG.A4LD	134.6	637.6	711.5	-0.06	9.7	1.62
TCSG.A4RD	46.3	586.1	766.5	-0.05	9.7	1.63
TCSG.B5RD	141.5	619.3	1322.2	0.14	9.7	1.86
TCSG.D5RD	51.4	1083.3	781.1	0.19	9.7	1.87
TCSG.E5RD	130.5	1221.9	669.9	0.20	9.7	1.87
TCSG.6RD	0.5	1668.3	236.8	0.25	9.7	2.55
TCLA.A6RD	90.0	1475.5	241.4	0.23	12.0	1.20
TCLA.B6RD	0.0	790.6	385.2	0.20	12.0	2.17
TCLA.C6RD	90.0	339.5	765.4	0.19	12.0	2.13
TCLA.D6RD	0.0	321.8	795.7	0.18	12.0	1.38
TCLA.A7RD	0.0	326.3	724.2	0.19	12.0	1.39
TCTs in IPG						
TCTH.4LG.H1	0.0	14699.2	24381.2	0.10	13.7	10.67
TCTVA.4LG.H1	90.0	14820.5	24794.2	0.10	13.7	13.86
Momentum cleaning						
TCP.6LJ	0.0	351.4	386.8	2.18	21.4	2.58
TCSG.5LJ	0.0	146.0	798.1	1.17	25.2	1.96
TCSG.4RJ	0.0	70.0	1055.7	-0.94	25.2	1.35
TCSG.A5RJ	170.8	95.8	919.3	-1.16	25.2	1.75
TCSG.B5RJ	11.4	121.7	835.3	-1.28	25.2	1.98
TCLA.A5RJ	90.0	381.0	470.3	-1.92	27.7	3.86
TCLA.B5RJ	0.0	405.3	450.7	-1.97	27.7	3.58
TCLA.6RJ	0.0	346.1	451.1	-1.28	27.7	3.31
TCLA.7RJ	0.0	180.0	239.0	1.16	27.7	2.39
TCTs in IPA						
TCTH.4LA.H1	0.0	14696.5	24381.4	0.10	13.7	10.67
TCTVA.4LA.H1	90.0	14817.8	24794.4	0.10	13.7	13.86

Table B.9: Description and location of FCC magnet classes.

Element Name	**Location**	**Location**
Dipoles		
MB	Main dipole	Arc
MBW	Warm dipole	ESS-D, ESS-J
MBXA.A	Recombination dipole, IP side (D1), module A	IPA, IPG
MBXA.B	Recombination dipole, IP side (D1), module B	IPA, IPG
MBRD.A	Recombination dipole, non-IP side (D2), module A	IPA, IPG
MBRD.B	Recombination dipole, non-IP side (D2), module B	IPA, IPG
Quadrupoles		
MQ	Main quadrupoles	Arc
MQW	Warm quadrupole	ESS-D, ESS-J
MQTL	Collimation insertion matching quadrupole (type A)	ESS-D, ESS-J
MQTLH	Collimation insertion matching quadrupole (type B)	ESS-D, ESS-J
MQY	IR matching wide-aperture quadrupole 6.8 m	IPA, IPG
MQML	IR matching quadrupole 9.6 m	IPA, IPG
MQM	IR matching quadrupole 6.8 m	IPA, IPG
MQX1	Triple magnet, IP side (Q1)	IPA, IPG
MQX2	Triplet magnet, central (Q2)	IPA, IPG
MQX3	Triplet magnet (Q3)	IPA, IPG
Kicker and Septa		
MKD	dump kicker	ESS-D
MSD	dump septum	ESS-D

Table B.10: Aperture parameters for the FCC magnet classes: inner dimensions of the vacuum chamber and mechanical tolerances split into radial, horizontal and vertical components. For some magnet classes, indicated by (1), the horizontal and vertical dimensions of the vacuum chamber can be inverted, according to the beam screen orientation. For the magnets in the inner triplet, indicated by (2), the mechanical tolerance is 0.0 in the crossing plane and different from 0.0 in the separation plane.

Element	**Vacuum chamber [mm]**		**Mech. tolerances [mm]**		
	h	v	r	h	v
Dipoles					
MB	15.0	13.2	1.65	1.1	0.0
MBW	29.5	22.0	0.84	2.1	1.4
MBXA.A	50.0	50.0	0.84	2.36	2.0
MBXA.B	53.0	53.0	0.84	2.36	2.0
MBRD.A	30.0	30.0	0.84	2.36	2.0
MBRD.B	22.0	22.0	0.84	2.36	2.0
Quadrupoles					
MQ	15.0	13.2	1.14	0.9	0.0
MQW	26.1	15.3	0.84	0.44	0.22
MQTL	15.0	13.2	0.84	0.94	0.62
MQTLH	15.5	13.7	0.84	1.31	0.85
(1)MQY	28.9	24.0	0.84	1.0	0.5
(1)MQML	15.5	13.7	0.84	1.0	0.5
MQM	15.0	13.2	0.84	1.0	1.0
MQX1	75.9	75.9	1.3	1.0	1.0
(2)MQX2	100.3	100.3	0.9	0.0/0.6	0.6/0.0
(2)MQX3	100.3	100.3	1.1	0.0/0.8	0.8/0.0
Kicker and Septa					
MKD	28.5	28.5	0.5	0.0	0.0
MSD	28.3	28.3	0.84	1.36	1.0